OPTICAL ENHANCEMENT AND ULTRAFAST EXCITON DYNAMICS IN HALIDE DOUBLE PEROVSKITES

RACHNA

DEPARTMENT OF CHEMISTRY

INDIAN INSTITUTE OF TECHNOLOGY DELHI

JANUARY 2025

OPTICAL ENHANCEMENT AND ULTRAFAST EXCITON DYNAMICS IN HALIDE DOUBLE PEROVSKITES

by

RACHNA

DEPARTMENT OF CHEMISTRY

Submitted

in fulfillment of the requirements of the degree of Doctor of Philosophy

to the

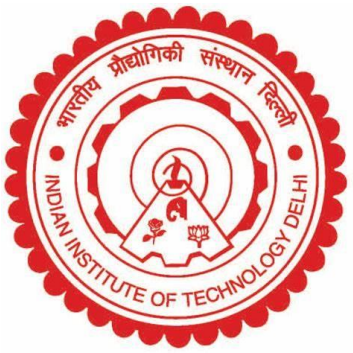

INDIAN INSTITUTE OF TECHNOLOGY DELHI

JANUARY 2025

Dedicated to

My Family

CERTIFICATE

This is to certify that the thesis entitled, "**Optical Enhancement and Ultrafast Exciton Dynamics in Halide Double Perovskites**" being submitted by **Ms. Rachna** to the **Indian Institute of Technology Delhi** for the award of the degree of **Doctor of Philosophy** in Chemistry, is a record of Bonafide research work carried out by her. Ms. Rachna has worked under my guidance and supervision.

Every time the study presented is based on the findings of other researchers, proper acknowledgement has been made in accordance with the standard procedure for publishing scientific observations. Any omission that may have resulted from a mistake or a lack of judgement is regrettable.

PROF. SAMEER SAPRA

Professor

Department of Chemistry

Indian Institute of Technology Delhi

New Delhi-110016

Acknowledgements

This PhD journey has been an unforgettable experience in my life, not only due to the challenging times and the obstacles I faced within my research project but because of all warm and loving memories I hold in my heart. Through it all, I learned, grew, and improved, and I'm immensely grateful to all the incredible people I encountered along the way.

First and foremost, I would like to express my heartfelt gratitude to my Ph.D. Supervisor, *Prof.* ***Sameer Sapra***. Your boundless patience, kindness, and knowledge are truly inspiring. It has been a privilege to work alongside you, and I look forward to many more rewarding years together. I also want to specially thank *Prof. Pramit K. Chowdhury* for teaching me about ultrafast transient spectroscopy, which broadened my understanding of ultrafast laser-based techniques during my research. My sincere gratitude goes out to all our wonderful and esteemed collaborators. I sincerely appreciate *Prof. Pralay K. Santra* for helping in transmission electron microscopic characterization, data analysis and scientific discussions. I would like to thank *Prof. Dibyajyoti Ghosh* for supporting us in theoretical calculations.

I express my deep sense of gratitude to past and present heads of our department *Prof. Ravi Shankar, Prof. Ashok K. Ganguly, Prof. Anil J. Elias, Prof. Narayanan D. Kurur, Prof. Siddharth Pandey and Prof. S. Nagendran* for providing all the necessary facilities in the department. I would like to take this opportunity to thank SRC members *Prof. P. P. Ingole, Prof. Samaresh Das* and *Prof. Pramit K Chowdhury* for their encouragement and constant support and review of my progress in PhD. I wish to convey my sincere thanks to *Prof. Sasanka Deka* and *Prof. Sayan Bhattacharya* for being an external assessment committee member for my senior research fellowship.

The Central Research Facility (CRF) and Nanoscale Research Facility (NRF) at IIT Delhi, as well as the *Sophisticated Analytical and Technical Help Institute (SATHI)* Foundation IIT

Delhi, have provided me with a wide range of characterization techniques that have been invaluable to the success of my research. I'd like to express my gratitude to everyone who's worked in the office or the instrumentation lab for their assistance with all administrative or scientific tasks. I express my sincere gratitude to the *Counsel of Scientific & Industrial Research (CSIR), India,* for PhD fellowship, which has made my PhD possible at IIT Delhi.

It's been a pleasure sharing the joys and challenges with my lab mates— *Dr. Md. Samim Hassan, Raman, Isha, Priyesh, Sahil, Swati, Varsha, Jyoti, Twinkle, Sagar, Ritu, Nitish and Deepak*.

I appreciate the post-doc fellows' sharing of their experiences, especially *Dr. Arkajyoti Chakrabarty, Dr. Jitendra Kumar, Dr. Sushma Yadav, Dr. Rajyashree* and *Dr. Umesh Yadav*. Special thanks to *Dr. Ajeet Singh* for encouraging me to take risks and make the best of available resources; for valuing my ideas and contributing to them. I like to appreciate my junior *Shubham* who was always there to help and kept me cheerful in tough times. My friends *Kriti*, *Vaishali*, and *Anu* are my all-time blessings, with whom I can express my grief and celebrate my happiness. Thanks to them for always being there for me. I am also indebted to the members of the other groups—particularly *Shubhangi and Deepika*—for generously sharing equipment and ideas.

Lastly, I owe my deepest gratitude to *my parents* for their constant encouragement, patience and trust over the years. Their boundless support and understanding, which has been instrumental in both my life and studies.

Finally, I would like to apologize if I have missed mentioning anyone and extend my heartfelt thanks to everyone who contributed to the successful completion of this thesis.

RACHNA

ABSTRACT

Lead-free halide double perovskites (HDPs) have recently emerged as promising candidates for optoelectronic applications, such as photovoltaics and light-emitting devices, owing to their tunable bandgaps, enhanced stability, and environmentally benign, non-toxic compositions. Despite these advantages, their practical deployment in light-based applications is hindered by the challenge of low photoluminescence quantum yields (PLQYs). To address this limitation, this thesis focuses on developing strategies to enhance the optical properties of lead-free HDPs. This thesis explores techniques aimed at improving the optical performance of these materials and investigates the ultrafast carrier dynamics through an integrated approach combining advanced experiments and characterization methods. The study places particular emphasis on elucidating the photophysical mechanisms underpinning exciton generation, recombination, and transport. By providing a detailed understanding of these processes, the thesis seeks to establish pathways for optimizing PLQY and advancing the potential of lead-free HDPs in next-generation optoelectronic devices.

The thesis is organized into seven chapters, where in **Chapter 1** we have provided a thorough overview of lead-free HDPs, outlining both their benefits and drawbacks. Here, we also concentrated on outlining the issue that this thesis aims to address. **Chapter 2** extends the discussion by elaborating on the analytical techniques employed to characterize the synthesized materials. This chapter provides a detailed exploration of the underlying principles, theoretical frameworks, and operational methodologies of these techniques, offering a comprehensive understanding of their application and relevance in material characterization. In **chapter 3** we used precise incorporation of Al^{3+} ions into the $Cs_2AgInCl_6$ lattice structure which facilitated a controlled modulation of the bandgap, resulting in a red shift in excitation energy. This adjustment not only optimized the material's optical properties but also significantly enhanced

self-trapped exciton (STE) emission, highlighting the effectiveness of Al doping in improving luminescent performance. The introduction of Al^{3+} contributed to a pronounced increase in electron-phonon coupling, as well as a higher density of STE states. Detailed cryogenic photoluminescence measurements shed light on the inhomogeneous nature of STE emission, revealing the presence of defect states that contribute to the variability in emission properties. Femtosecond transient absorption (fs-TA) spectroscopy provided a comprehensive understanding of the dynamics of charge carrier trapping. PLQY of $Cs_2AgInCl_6$ is increased up to ~8%. In **chapter 4** we used Bi^{3+} as the dopant instead of Al^{3+} in $Cs_2AgInCl_6$. We synthesized different doped amount of $Cs_2AgIn_{(1-x)}Bi_xCl_6$. We find the effect of this doping on the structural and optical properties of host lattice. We tried to unveil the factors responsible for the changes we observed using different techniques. It was observed that Bi provide symmetry breakdown to the electronic structure of $Cs_2AgInCl_6$ and increases the absorbance. Bandgap changes reveal the Bi convert the direct bandgap to indirect. Extent of electron phonon coupling is determined to understand the reason of increase in PLQY up to ~ 40%. In **chapter 5**, After establishing the role of Bi^{3+} we incorporated Sm^{3+} to introduce the sharp and narrow emission in the visible region originating from the f-f transition. Bi-doped $Cs_2AgInCl_6$ NCs were found to be better host for sensitized f-f transitions and resulted in the enhanced PLQY. In **chapter 6**, we developed a new synthesis strategy to realize the $Cs_2AgBiCl_6$@$Cs_2NaInCl_6$ core@shell nano heterostructures with enhanced PLQY. The epitaxial growth of $Cs_2NaInCl_6$ over $Cs_2AgBiCl_6$ is monitored by comparing the structural and optical changes. The detailed morphology characterization was employed to successfully prove the presence of two component is one nano crystallite. Pl intensity is found to be increased by 10-fold in the heterostructure. The carrier dynamics was also studied using ultrafast lifetime characterisation. **Chapter 6** describes the summary of complete thesis and provide some innovative ideas which can be looked upon for future studies in the field of these lead-free HDPs.

सारांश

Pb-फ्री हैलाइड डबल पेरोवस्काइट्स (एचडीपी) हाल ही में ऑप्टोइलेक्ट्रोनिक अनुप्रयोगों के लिए आशाजनक उम्मीदवारों के रूप में उभरे हैं, जैसे कि फोटोवोल्टिक्स और प्रकाश उत्सर्जक उपकरण, कारण उनके ट्यून करने योग्य बैंडगैप्स, बढ़ी हुई स्थिरता और पर्यावरणीय रूप से सौम्य, गैर विषाक्त रचना है। इन फायदों के बावजूद, प्रकाश-आधारित अनुप्रयोगों में उनकी व्यावहारिक तैनाती कम फोटोल्यूमिनेसेंस क्वांटम (PLQY) पैदावार की चुनौती से बाधित है। इस सीमा को संबोधित करने के लिए, यह थीसिस Pb रहित एचडीपी के ऑप्टिकल गुणों को बढ़ाने के लिए रणनीतियों को विकसित करने पर केंद्रित है। यह थीसिस इन सामग्रियों के ऑप्टिकल प्रदर्शन में सुधार लाने के उद्देश्य से तकनीकों की पड़ताल करती है और उन्नत प्रयोगों और लक्षण वर्णन विधियों के संयोजन के माध्यम से एक एकीकृत दृष्टिकोण के माध्यम से अल्ट्राफास्ट वाहक गतिशीलता की जांच करती है। अध्ययन में exciton उत्पादन, पुनर्संयोजन और परिवहन को रेखांकित करने वाले फोटोफिजिकल तंत्र को स्पष्ट करने पर विशेष जोर दिया गया है। इन प्रक्रियाओं की विस्तृत समझ प्रदान करके, थीसिस PLQY को अनुकूलित करने और अगली पीढ़ी के ऑप्टोइलेक्ट्रॉनिक उपकरणों में Pb रहित एचडीपी की क्षमता को आगे बढ़ाने के लिए मार्ग स्थापित करना चाहती है।

थीसिस को सात अध्यायों में व्यवस्थित किया गया है, जहां **अध्याय 1** में हमने Pb रहित एचडीपी का गहन अवलोकन प्रदान किया है, जो उनके लाभ और कमियां दोनों को रेखांकित करता है। यहां, हमने इस मुद्दे को रेखांकित करने पर भी ध्यान केंद्रित किया कि इस थीसिस का उद्देश्य संबोधित करना है। **अध्याय 2** संश्लेषित सामग्री को चिह्नित करने के लिए नियोजित विश्लेषणात्मक तकनीकों पर विस्तार से चर्चा करता है। यह अध्याय इन तकनीकों के अंतर्निहित सिद्धांतों, सैद्धांतिक रूपरेखाओं और परिचालन पद्धतियों का विस्तृत अन्वेषण प्रदान करता है, जो सामग्री लक्षण वर्णन में उनके आवेदन और प्रासंगिकता की व्यापक समझ प्रदान करता है। **अध्याय 3** में हमने $Cs_2AgInCl_6$ नैनोक्रिस्टल में Al^{3+} आयनों के सटीक समावेश

का उपयोग किया, जिसने बैंडगैप के नियंत्रित मॉड्यूलेशन की सुविधा प्रदान की, जिसके परिणामस्वरूप उत्तेजना ऊर्जा में लाल बदलाव हुआ। इस समायोजन ने न केवल सामग्री के ऑप्टिकल गुणों को अनुकूलित किया, बल्कि STEs को भी काफी बढ़ाया, जो ल्यूमिनसेंट प्रदर्शन में सुधार करने में Al^{3+} डोपिंग की प्रभावशीलता को उजागर करता है। Al^{3+} की शुरूआत ने इलेक्ट्रॉन-फोनन युग्मन में स्पष्ट वृद्धि के साथ-साथ STEs के उच्च घनत्व में योगदान दिया। विस्तृत क्रायोजेनिक फोटोल्यूमिनेसेंस माप STE उत्सर्जन की अमानवीय प्रकृति पर प्रकाश डालते हैं, जिससे उत्सर्जन गुणों में परिवर्तनशीलता में योगदान देने वाले दोष राज्यों की उपस्थिति का पता चलता है। फेमटोसेकंड स्पेक्ट्रोस्कोपी ने चार्ज कैरियर ट्रैपिंग की गतिशीलता की व्यापक समझ प्रदान की। $Cs_2AgInCl_6$ की PLQY ~ 8% तक बढ़ जाती है। **अध्याय 4** में हमने $Cs_2AgInCl_6$ में Al^{3+} के बजाय Bi^{3+} को डोपेंट के रूप में उपयोग किया। हमने $Cs_2AgIn_{(1-x)}Bi_xCl_6$ की विभिन्न डोप्ड मात्रा को संश्लेषित किया। हम $Cs_2AgInCl_6$ के संरचनात्मक और ऑप्टिकल गुणों पर इस डोपिंग का प्रभाव पाते हैं। हमने विभिन्न तकनीकों का उपयोग करके देखे गए परिवर्तनों के लिए जिम्मेदार कारकों का अनावरण करने की कोशिश की। यह देखा गया कि Bi $Cs_2AgInCl_6$ की इलेक्ट्रॉनिक संरचना को समरूपता विखंडन प्रदान करता है और अवशोषण को बढ़ाता है। बैंडगैप परिवर्तन से पता चलता है कि Bi^{3+} प्रत्यक्ष बैंडगैप को अप्रत्यक्ष में परिवर्तित करता है। इलेक्ट्रॉन फोनन युग्मन की सीमा ~ 40% तक PLQY में वृद्धि के कारण को समझने के लिए निर्धारित की जाती है। **अध्याय 5** में, Bi^{3+} की भूमिका स्थापित करने के बाद हमने f-f संक्रमण से उत्पन्न होने वाले दृश्य क्षेत्र में तेज और संकीर्ण उत्सर्जन को पेश करने के लिए Sm3+ को शामिल किया। द्वि-मिश्रित $Cs_2AgInCl_6$ NCs को संवेदनशील f-f संक्रमणों के लिए बेहतर मेजबान पाया गया और इसके परिणामस्वरूप PLQY में वृद्धि हुई। **अध्याय 6** में, हमने उन्नत PLQY के साथ $Cs_2AgBiCl_6$@$Cs_2NaInCl_6$ core@shell नैनो हेटरोस्ट्रक्चर का एहसास करने के लिए एक नई संश्लेषण रणनीति विकसित की। $Cs_2AgBiCl_6$ पर $Cs_2NaInCl_6$ की एपिटैक्सियल वृद्धि की निगरानी संरचनात्मक और ऑप्टिकल परिवर्तनों की तुलना करके की जाती है। विस्तृत आकृति विज्ञान लक्षण वर्णन सफलतापूर्वक दो घटक एक नैनो क्रिस्टलीय है की

उपस्थिति साबित करने के लिए नियोजित किया गया था. विषमसंरचना में फोटोल्यूमिनेसेंस 10 गुना बढ़ी हुई पाई जाती है। वाहक गतिशीलता का अध्ययन अल्ट्राफास्ट जीवनकाल लक्षण वर्णन का उपयोग करके भी किया गया था। **अध्याय 6** पूर्ण थीसिस के सारांश का वर्णन करता है और कुछ नवीन विचार प्रदान करता है जिन्हें इन सीसा रहित एचडीपी के क्षेत्र में भविष्य के अध्ययन के लिए देखा जा सकता है।

Table of Contents

Certificate……..iii
Acknoledgements……..……....iv
Abstract..…….vi
सारांश……...viii
List of Figures……..xv
List of Tables……...xxi
Glossary of abbreviations and acronyms……xxii

Chapter 1 1

1.1 Emergence of halide double perovskites 1

1.2 Features of Lead- free halide double Perovskites..... 4

1.2.1 Compositional and Structural flexibility..... 4

1.2.2 Electronic Structure 4

1.2.3 Optical properties..... 7

1.2.4 Defect Tolerance 13

1.2.5 Stability 16

1.2.6 Environment Friendliness 17

1.3 Challenges and Drawbacks of lead-free HDPs 18

1.3.1 Wide and Indirect Band Gap 18

1.3.2 Parity Forbidden Transitions 20

1.3.3 Low PLQY 20

1.4 Aim of Present Work 21

Chapter 2 24

2.1 Nanocrystal Synthesis..... 25

2.2 Structural Characterization..... 26

2.2.1 Powder X-Ray Diffraction 26

2.2.2 Transmission Electron Microscopy 28

2.2.3 X-Ray Photoelectron Spectroscopy..... 30

2.3 Optical Characterization 31

2.3.1 Inductively Coupled Plasma Optical Emission Spectroscopy 31

2.3.2 UV/VIS Absorption spectroscopy 32

2.3.3 Steady State Photoluminescence Spectroscopy 33
2.3.4 Time-resolved Photoluminescence Spectroscopy 35
2.3.5 Absolute Photoluminescence quantum yield 38
2.3.6 Ultrafast Transient Absorption Spectroscopy 39
2.3.7 Raman Spectroscopy 41
Chapter 3 42
3.1 Introduction 43
3.2 Materials and Experimental Methods 44
3.2.1 Materials 44
3.2.2 Experimental Methods 44
3.2.3 Characterization Techniques 45
3.3 Result and Discussion 47
3.3.1 Powder X-Ray Diffraction 47
3.3.2 Raman Spectroscopy 51
3.3.3 Transmission Electron Microscopy 52
3.3.4 X-Ray Photoelectron Spectroscopy 53
3.3.5 Steady-State Absorption and Photoluminescence Spectroscopy 54
3.3.6 Temperature dependent Photoluminescence Spectroscopy 57
3.3.7 Fs- Transient Absorption Spectroscopy 62
3.4 Conclusion 67
Chapter 4 69
4.1 Introduction 70
4.2 Materials and Experimental Methods 71
4.2.1 Materials 71
4.2.2 Experimental Methods 71
4.2.3 Characterization techniques 72
4.3 Results and Discussion 74
4.3.1 Powder X-Ray Diffraction 75
4.3.2 Raman Spectroscopy 77

4.3.3 Transmission Electron Microscopy 78
4.3.4 X-Ray Photoelectron Spectroscopy 79
4.3.5 Absorbance and Photoluminescence Spectroscopy 82
4.3.6 fs-Transient Absorption Spectroscopy 88
4.4 Conclusion 90
Chapter 5 91
5.1 Introduction 92
5.2 Materials and Experimental Methods 94
5.2.1 Materials 94
5.2.2 Experimental Methods 94
5.2.3 Characterization Techniques 95
5.3 Result and discussion 97
5.3.1 Powder X-Ray Diffraction 98
5.3.2 X/ray Photoelectron Spectroscopy 102
5.3.3 Transmission Electron Microscopy 103
5.3.4 Raman Spectroscopy 105
5.3.5 Absorption and Photoluminescence Spectroscopy 106
5.3.6 fs-Transient Absorption Spectroscopy 113
5.4 Conclusion 116
Chapter 6 117
6.1 Introduction 118
6.2 Material and Experimental Methods 120
6.2.1 Materials 120
6.2.2 Experimental Methods 120
6.2.3 Characterization techniques 121
6.3 Results and Discussion 122
6.3.1 Powder X-Ray Diffraction 122
6.3.2 Transmission Electron Microscopy 125
6.3.3 X-Ray Photoelectron Spectroscopy 128

6.3.4 Absorption and Photoluminescence Spectroscopy 129
6.3.5 fs-Transient Absorption Spectroscopy 131
6.3.6 Structural and optical stability data 135
6.4 Conclusion 136
Chapter 7 137
7.1 Summary 137
7.2 Major Advances of the thesis work 138
7.3 Future Scope 139
Bibliography 149
Bio-Data 183

List of Figures

Chapter 1

Figure 1.1: *Types of perovskite structures resulted from cation transmutation in ABX_3 perovskite.* *3*

Figure 1.2: *Calculated electronic band structures of* ***(a)*** *$Cs_2AgBiCl_6$ and* ***(b)*** *$Cs_2AgInCl_6$. Adapted with permission from reference [54].* *6*

Figure 1.3: *Schematic of molecular orbital diagram showing bonding and anti-bonding bands of (a) $Cs_2AgInCl_6$ and (b) $Cs_2AgBiCl_6$. Adapted with permission from references [57 58]* .. *7*

Figure 1.4: *Types of electrons and hole recombination mechanism. Adapted with permission from reference [60]* *8*

Figure 1.5: *Schematic of intrinsic self-trapping of exciton by local minima formation in lattice due to electron phonon coupling.* *8*

Figure 1.6: *Non radiative pathways for phonon assisted recombination.* *10*

Figure 1.7: *Electronic transitions of Bi^{3+} ions after photoexcitation.* *12*

Figure 1.8: *Electronic structure of conventional defect intolerant semiconductors (left) compared to the defect tolerant LHP crystal structure (right). Adapted with permission from [80]* *14*

Figure 1.9: *Parity forbidden and allowed transitions in $Cs_2AgInCl_6$. Adapted with permission from [106]* *20*

Chapter 2

Figure 2.1: *Schematic diagram of NCs with "hot injection" synthesis approach using Schlenk line setup.* *25*

Figure 2.2: *Schematic representation of (a) a traditional x-ray tube and (b) Copper characteristic transitions for X rays.* *26*

Figure 2.3: *Schematic illustration of phenomenon of X-ray diffraction by atomic planes and derivation of Bragg's law..... 27*

Figure 2.4: *Schematic of TEM instrument. Adapted with permission from [123]..... 29*

Figure 2.5: *Schematic diagram of ICP-OES. Adapted with permission from [125] 31*

Figure 2.6: *Jablonski diagram showing electronic transitions and luminescent process time scales. Adapted with permission from [127] 34*

Figure 2.7: *Mechanism of TCSPC. Adapted with permission from [126] 37*

Figure 2.8: *Schematic for PLQY measurements. Adapted with permission from [130] 38*

Figure 2.9: *Schematic of fs-TA instrument and data. 40*

Chapter 3

Figure 3.1: (a) *Schematic of the synthesis methodology of Al^{+3} doped $Cs_2AgInCl_6$ NCs* ***(b)*** *PXRD patterns of $Cs_2AgIn_{1-x}Al_xCl_6$ (x = 0, 0.005, 0.01, 0.03, 0.05) compared with standard diffraction pattern of $Cs_2AgInCl_6$ (ICSD#19130), the enlarged peak of (220) indicates the negligible shift in XRD pattern with the increased Al^{3+} concentration* ***(c)*** *Raman spectra of $Cs_2AgIn_{1-x}Al_xCl_6$ NCs and magnified Raman modes,* ***(d, g)*** *TEM images,* ***(e, h)*** *HRTEM images,* ***(f, i)*** *SAED patterns of Al:0 and Al:5 respectively. 48*

Figure 3.2: *Rietveld refinement of XRD patterns of $Cs_2AgIn_{(1-x)}Al_xCl_6$ NCs with respect to the standard CIF file of $Cs_2AgInCl_6$. 49*

Figure 3.3: (a) *Cell parameter as a function of doped amount of Al^{3+}* ***(b)*** *FWHM of (220) diffraction plane for $Cs_2AgIn_{(1-x)}Al_xCl_6$ NCs. 51*

Figure 3.4: *TEM images and corresponding size distributions of $Cs_2AgIn_{(1-x)}Al_xCl_6$ DP NCs. 52*

Figure 3.5: *(a) Survey XPS spectrum of Al:0 and Al:1. (b-f) high resolution XPS spectrum of Cs^+ 3d, Ag^+ 3d, In^{3+} 3d, Cl 2p and Al^{3+} 2s for Al 1. ..... 54*

Figure 3 6: (a) *Absorbance spectra of $Cs_2AgIn_{1-x}Al_xCl_6$ NCs in hexane solution* ***(b)*** *Tauc plots of band edge transition of $Cs_2AgInCl_6$ NCs with different Al^{3+} doping concentration* ***(c)*** *Excitation spectra of $Cs_2AgIn_{1-x}Al_xCl_6$ NCs in hexane solution corresponding to* ***(d)*** *the broad emission located around 600 nm.* ***(e)*** *Time resolved PL spectra of $Cs_2AgIn_{1-x}Al_xCl_6$ NCs at room temperature.* ***(f)*** *PLQY (λ_{exc} = 290 nm) and average lifetime of broad emission as a function of Al^{3+} doping concentration..... 55*

Figure 3.7: *Decay profiles of $Cs_2AgIn_{(1-x)}Al_xCl_6$ NCs at 600 nm emission in μs time scale.. 56*

Figure 3 8: *Temperature-dependent PL emission spectra (λex = 310 nm) of* ***(a)*** *Al:0 and* ***(b)*** *Al:1 in the temperature range of 10 − 300 K. FWHM of the STE emission in of* ***(c)*** *Al:0 and Al:1 as a function of temperature. Huang-Rhys factor (S), and the phonon energy ($\hbar\omega phonon$) of the crystal lattice were derived by fitting to the data in* ***(a)−(b)****.* ***(d)*** *The schematic of emission mechanism of DP $Cs_2AgInCl_6$ at low and high temperature. 59*

Figure 3.9: *PL Intensity dependence of Al:0 and Al:1at different temperature. Arrhenious equation: ln I(T) v/s 1/T plot..... 60*

Figure 3.10: *Temperature dependent deconvoluted PL emission of (a-e) Al:0 and (f-j) Al:1. 61*

Figure 3.11: *PL kinetics of Al:1 at different emission wavelength showing STE behavior around 600..... 62*

Figure 3.12: *Contour plots of the fs-TA spectra of* ***(a)*** *Al:0 and* ***(d)*** *Al:1 upon excitation with a 300 nm fs-pulsed laser. Spectral profiles of fs-TA spectra of* ***(b)*** *Al:0 and* ***(e)*** *Al:1 at different delay times. Normalized PIA decay curves of* ***(c)*** *Al:0 and* ***(f)*** *Al:1 probed at different wavelengths. 63*

Figure 3.13: *TA Spectral profile and Kinetic profiles of Al 0 and Al 1 within sub ps range. Immediate results after excitation..... 65*

Figure 3.14: *Configuration coordinate diagram of $Cs_2AgInCl_6:Al^{3+}$, showing quantization of STE energy levels and the involved electronic transitions. GS and FE denote the ground state and FE, respectively. 67*

Chapter 4

Figure 4.1: *(a) PXRD patterns of $Cs_2AgIn_{(1-x)}Bi_xCl_6$, (b) change in cell parameter with respect to doping concentration of Bi^{3+} and (c) Raman spectra of $Cs_2AgIn_{(1-x)}Bi_xCl_6$..... 75*

Figure 4.2: *Rietveld refinement plots for XRD patterns of $Cs_2AgIn_{(1-x)}Bi_xCl_6$ NCs fitted with respect to standard pattern of $Cs_2AgInCl_6$ 76*

Figure 4.3: *TEM images of Bi:0, Bi:1, Bi:10, Bi:50, Bi:100 with HRTEM images in the insets (upper panel) and size distribution histograms (lower panel) 79*

Figure 4.4: *high resolution XPS spectrum of all the elements in(a-d) Bi:0 and (e-i) Bi:1..... 81*

Figure 4.5: *(a) Absorbance (dotted line), PLE (solid line) and PL (shaded area) (b) PLQY, (c) Kinetic profile of PL decay at 650 nm and (d) average lifetime with respect to doping percentage of Bi^{3+}. 82*

Figure 4.6: *Decay profiles of Bi:0.5 at different emission wavelength in time range of (a) 15μs (b) 100 ns and (c) 4ns. 85*

Figure 4.7: *(a) Direct bandgap (b) Indirect bandgap of $Cs_2AgIn_{(1-x)}Bi_xCl_6$ using Tauc plot, (c) change in bandgap energy with respect to doped Bi^{3+} and (d) temperature dependent change in FWHM of PL in Bi:0, Bi:0.5 and Bi:100..... 86*

Figure 4.8: *3D pseudo color plots of the fs-TA spectra of **(a)** Bi:0 and **(d)** Bi:0.5 upon excitation with a 300 nm fs-pulsed laser. TA spectra of **(b)** Bi:0 and **(e)** Bi:0.5 at different delay times. PIA kinetic data of **(c)** Bi:0 and **(f)** Bi:0.5 probed at different wavelengths. 89*

Chapter 5

Figure 5.1: *(a) Synthesis scheme for the cubic NCs of $Cs_2Ag(In_{1-x}Sm_x)Cl_6$:Bi (b) XRD patterns of $Cs_2Ag(In_{1-x}Sm_x)Cl_6$:Bi NCs and magnified 220 diffraction peak, (c) dependence of refined cell parameter of $Cs_2Ag(In_{1-x}Sm_x)Cl_6$:Bi NCs with Sm^{3+} doping proportion. 99*

Figure 5.2: *Powder XRD patterns of DP:U0, DP:S5.6 and DP:rev..... 100*

Figure 5.3: *Rietveld refinement of XRD patterns of $Cs_2AgIn_{(1-x)}Sm_xCl_6$:Bi NCs with respect to standard pattern CIF file of $Cs_2AgInCl_6$ 101*

Figure 5.4: *PXRD patterns of $Cs_2AgIn_{(1-x)}Sm_xCl_6$:Bi NCs with higher percentages of Sm^{3+}showing the presence of impurity phases. 102*

Figure 5.5: *(a) Survey XPS spectrum of DP:U0, DP:S0 and DP:S4.1. (b-f) high resolution XPS spectrum of Cs^+ 3d, Ag^+ 3d, In^{3+} 3d, Cl 2p and Sm^{3+} 3d for DP:S4.1..... 102*

Figure 5.6: *High resolution XPS spectrum of all elements Cs3d, Ag3d, In3d and Cl2p in DP:U0. ..... 103*

Figure 5.7: (a, e) *TEM images,* ***(b, f)*** *HRTEM images,* ***(c, g)*** *SAED patterns* ***(d, h)*** *TEM histograms of DP:U0 and DP:S8.2 respectively..... 104*

Figure 5.8: *low resolution TEM images of $Cs_2AgIn_{(1-x)}Sm_xCl_6$:Bi DP NCs. 105*

Figure 5.9: *Spectra (absorbance and PLE monitored at 604 nm – left and PL at 280 and 368 nm excitation-Right) for* ***(a)*** *DP:U0 and DP:S0, and* ***(b)*** *DP:U1.6 and DP:S1.9,* ***(c)*** *absorbance and PLE monitored at 604 nm (left) and PL spectra excited by 368 nm (right) for all DP NCs.* ***(d)*** *PL intensity comparison of STE emission at ~540 nm and Sm^{3+} emission for corresponding NCs.* ***(e)*** *Raman spectra of undoped, Bi^{3+} doped and Bi^{3+}/Sm^{3+} codoped NCs. 107*

Figure 5.10: *PL spectra of $Sm(NO_3)_3.6H_2O$. 108*

Figure 5.11: (a) *STE contribution in PL and* ***(b)*** *PL intensity of separated Sm^{3+} emission. .110*

Figure 5.12: (a) *PL decay curves of STEs emission from corresponding samples monitored at 520 nm emission.* ***(b)*** *average decay time constants of STE emission monitored at 520 nm*

(left) and energy transfer efficiency from STE states to Sm^{3+}. ***(c,d)*** *fs TA contour plots of DP:S0 and DP:S4.1* ***(e)*** *PIA decay dynamics of DP:S0 and DP:S4.1 probed at 610 nm* ***(f)*** *Luminescence mechanism of Bi^{3+} and Sm^{3+} codoped $Cs_2AgInCl_6$ NCs. 111*

Figure 5.13: *Spectral profile at different delay times for* ***(a)*** *DP:S0 and* ***(b)*** *DP:S4.1.* ***(c)*** *kinetic curves of DP:S4.1 probed at different wavelengths. 113*

Figure 5.14: *Structural and optical features of $Cs_2AgIn_{(1-x)}Sm_xCl_6$:Bi NCs collected after four months. 115*

Figure 5.15: *Structural evolution in Bi^{3+} sensitized and unsensitized Sm^{3+} doped $Cs_2AgInCl_6$ NCs after four months. 116*

Chapter 6

Figure 6.1: *Schematic representation of stepwise synthesis of CABC@CNIC core@shell NCs. 121*

Figure 6.2: *(a) PXRD patterns of pure CABC, CNIC and CABC@CNIC NCs, refined XRD patterns of (b) pure CABC, (c) pure CNIC and (d) CABC@CNIC NCs. 123*

Figure 6.3: *TEM images of (a) pure CABC and (b) CABC@CNIC NCs (with size distribution in respective insets). 125*

Figure 6.4: *HRTEM image of a $Cs_2AgBiCl_6$ NC and corresponding Fourier transform pattern of the HRTEM image of selected particle. HAADF-STEM image and corresponding elemental mapping image showing the elemental distribution of all expected elements in $Cs_2AgBiCl_6$ NCs. (upper panel) and $Cs_2AgBiCl_6$@$Cs_2NaInCl_6$NCs. (lower panel) 127*

Figure 6.5: *(a-d) high resolution XPS spectra of CABC compared with respective element in CABC@CNIC, (e-h) high resolution XPS spectra of CNIC compared with respective element in CABC@CNIC. 128*

Figure 6.6: *(a) absorption spectra, (b) PLE spectra at 650 nm emission, PL spectrum at (c) 280 nm, (d) 340 nm, (e) 370 nm excitation and (f) lifetime data for pure CABC and CABC@CNIC NCs.* *130*

Figure 6.7: *(a) Absorbance spectrum of CABC and CABC@CNIC samples used for collection of TA spectrum. TA spectrum of (b) pure CABC, (c) CABC@CNIC at 290 nm pump excitation, (d) comparison of kinetic profile and (e) Normalized kinetic data of bleach recovery in pure CABC and CABC@CNIC, (f) comparison of kinetic profile and (g) Normalized kinetic data of PIA signal in pure CABC and CABC@CNIC.* *132*

Figure 6.8: *(a) XRD pattern of physical mixture of CABC and CNIC, (b) absorbance spectrum of physical mixture of CABC and CNIC, pure CABC and pure CNIC, (c) PLE spectrum of pure CABC and of physical mixture of CABC and CNIC corresponding to emission wavelength of 650 nm, (d) PL spectrum of physical mixture of CABC and CNIC, pure CABC and pure CNIC at excitation wavelength of 340 nm.* *134*

Figure 6.9: *Time dependent changes in (a) XRD pattern, (b) absorbance, (c) PLE spectrum and (d) PL spectrum of CABC@CNIC NCs.* *135*

List of Tables

Chapter 3

Table 3. 1: Al^{3+} content in $Cs_2AgIn_{(1-x)}Al_xCl_6$ NCs measured by ICP. 47

Table 3. 2: Rietveld Refinement parameters of PXRD patterns of $Cs_2AgInCl_6$:Al NCs..... 50

Table 3. 3: Parameters of Fitted lifetimes of $Cs_2AgIn_{1-x}Al_xCl_6$ NCs at 520 nm. 57

Table 3. 4: Fitting parameters of PIA kinetics probed at different wavelength for Al:0..... 66

Table 3. 5: Fitting parameters of PIA kinetics probed at different wavelength for Al:1..... 66

Chapter 4

Table 4. 1: Bi^{3+} content in $Cs_2AgIn_{(1-x)}Bi_xCl_6$ NCs measured by ICP 72

Table 4. 2: Rietveld refinement parameters for XRD patterns of $Cs_2AgIn_{(1-x)}Bi_xCl_6$ NCs 77

***Table 4. 3:** Fitting parameters of PL decay of $Cs_2AgIn_{(1-x)}Bi_xCl_6$ NCs measured at 650 nm emission 83*

***Table 4. 4:** Calculate radiative decay rates for STE in $Cs_2AgIn_{1-x}Bi_xCl_6$ NCs..... 84*

Table 4. 5: Fitting parameters of PL kinetics of Bi:0.5..... 85

Chapter 5

Table 5. 1: Sm^{3+} content in $Cs_2AgIn_{(1-x)}Sm_xCl_6$:Bi NCs measured by ICP..... 95

Table 5. 2: Rietveld Refinement parameters of PXRD patterns of $Cs_2AgIn_{(1-X)}Sm_XCl_6$:Bi NCs. 100

Table 5. 3: Parameters of Fitted lifetimes of $Cs_2AgIn_{1-x}Sm_xCl_6$:Bi NCs at 520 nm.....112

Table 5. 4: Fitting parameters of PIA decay kinetics probed at 610 nm.....114

Chapter 6

Table 6. 1: Rietveld refinement parameters of PXRD patterns of CABC and CNIC 124

Table 6. 2: Rietveld refinement parameters of PXRD pattern of CABC@CNIC..... 125

Table 6. 3: Fitting parameters of PL decay kinetics probed at 650 nm. 131

Glossary of Abbreviations and Acronyms

μ	octahedral factor
t	Goldschmidt tolerance factor
r_i	Ionic radii
LED	Light-Emitting Diodes
PLQY	Photoluminescence Quantum Yield
HDPs	Halide Double Perovskite
STEs	Self-trapped excitons
NC	Nanocrystals
LHP	Lead-halide perovskite
3D	Three Dimensional
RP	Ruddlesden–Popper
DP	Dion–Jacobson
DFT	Density functional theory
VASP	Vienna Ab initio Simulation Package
CBm	Conduction Band minima
VBM	Valance Band Maxima
ps	Picosecond
FWHM	Full-Width at Half-Maxima
TEM	Transmission Electron Microscopy
HRTEM	High Resolution Transmission Electron Microscopy
HAADF	High-Angle Annular Dark Field
ICP-OES	Inductively Coupled Plasma Optical Emission Spectroscopy
ODE	1,3- Octadecene
OlAm	Oleyl Amines
OA	Oleic Acid
TMSCl	Trimethylsilyl chloride
JCPDS	Joint Committee on Powder Diffraction Standards
CCD	Charge coupled device
SAED	Selected Area Electron Diffraction
TCSPC	Time-correlated single-photon counting
FE	Free excitons
GS	Ground State
ES	Excited State
GSB	Ground State Bleach
PIA	Photo Induced Absorption